Matter

CellPress

Article

Designing lattices for impact protection using transfer learning

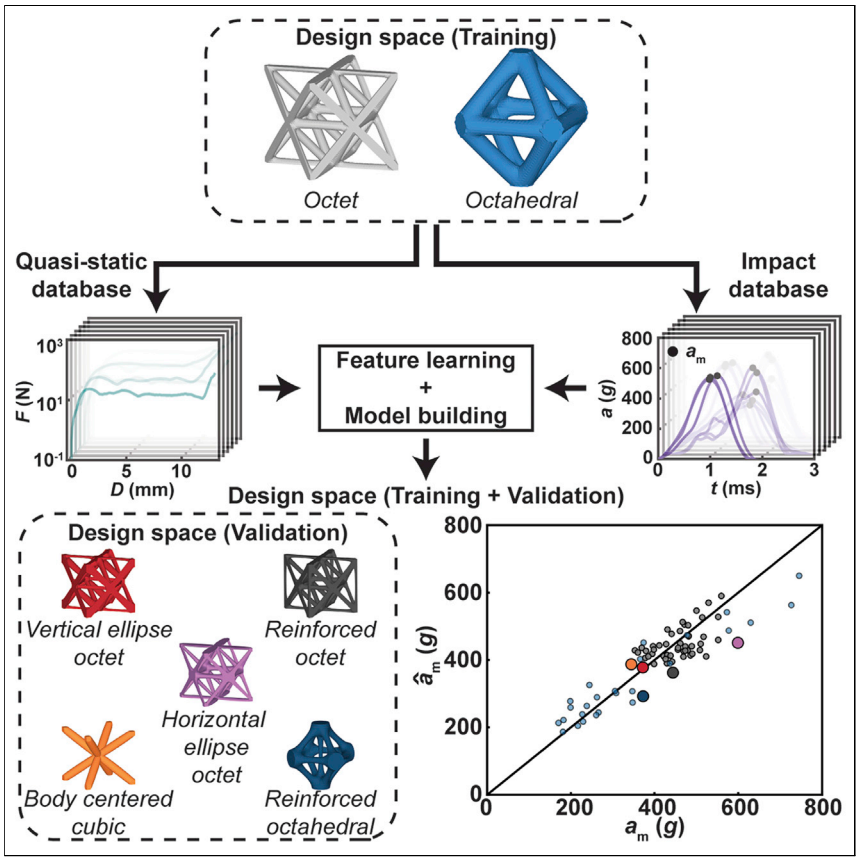

We report a transfer learning approach for using general testing to predict the specialized performance of 3D-printed lattices. Specifically, we curated a large dataset of quasi-static tests using automated testing and learned a general featurization. Next, we connected this featurization to experimentally measured impact performance and found that the model predicted the impact performance of novel lattice families with 18% error. These results show how design for specialty applications can be accelerated in a data-driven manner.

Aldair E. Gongora, Kelsey L. Snapp, Richard Pang, ..., Timothy J. Lawton, Elise F. Morgan, Keith A. Brown

efmorgan@bu.edu (E.F.M.)
brownka@bu.edu (K.A.B.)

Highlights

Novel families of 3D-printed lattices evaluated using automated mechanical testing

Machine-learning model predicts impact performance using quasi-static behavior

Lattices with optimized impact performance achieved using a data-driven approach

Illustrated how specialized performance can be transfer learned from general testing

3 Understanding
Dependency and conditional studies on material behavior

Gongora et al., Matter 5, 1–18
September 7, 2022
https://doi.org/10.1016/j.matt.2022.06.051

Please cite this article in press as: Gongora et al., Designing lattices for impact protection using transfer learning, Matter (2022), https://doi.org/10.1016/j.matt.2022.06.051

Matter

CellPress

Article

Designing lattices for impact protection using transfer learning

Aldair E. Gongora,[1] Kelsey L. Snapp,[1] Richard Pang,[2] Thomas M. Tiano,[2] Kristofer G. Reyes,[3] Emily Whiting,[4] Timothy J. Lawton,[2] Elise F. Morgan,[1,5,6,*] and Keith A. Brown[1,6,7,8,*]

SUMMARY

Like many specialty applications, the pace of designing structures for impact protection is limited by its reliance on specialized testing. Here, we develop a transfer learning approach to determine how more widely available quasi-static testing can be used to predict impact protection. We first extensively test a parametric family of lattices in both impact and quasi-static domains and train a model that predicts impact performance to within 8% using only quasi-static measurements. Next, we test the transferability of this model using a distinct family of lattices and find that performance rank was well predicted even for structures whose behavior extrapolated beyond the training set. Finally, we combine 812 quasi-static and 141 impact tests to train a model that predicts absolute impact performance of novel lattices with 18% error. These results highlight a path for accelerating design for specialty applications and that transferrable mechanical insight can be obtained in a data-driven manner.

INTRODUCTION

Structures for impact protection play a vital role in a plethora of applications ranging from padding used in defense to safety components used in the automotive and aerospace industries.[1–3] A common task is to minimize the acceleration experienced by a sensitive component during an impact event. However, designing high-performing structures for impact is challenging due to the required co-optimization of distinct properties including compliance, strength, and toughness.[1,2,4–7] With the advent of additive manufacturing (AM), unprecedented opportunities have emerged for fabricating novel designs with superior mechanical performance relative to their conventionally manufactured counterparts.[8–14] Lattices, such as the widely studied octet lattice, are one type of mechanical structure enabled by AM that have potential for impact protection as their cellular nature affords high specific energy absorption, and they exhibit a high degree of design flexibility. Nevertheless, rapidly traversing the vast AM design space to select optimal components is not currently possible. Traditional tools for rapid design such as finite element analysis (FEA) and topology optimization are not effective for predicting impact performance, as these approaches have limited fidelity for such measurements. These limitations stem from the material and geometric non-linearities, the dependence of material properties on strain rate, and dynamic self-collisions that are challenging to model for structures with complex architectures.[3,14,15] Thus, design of structures for impact performance necessitates physical experimentation that leads to low-throughput iterative design.

Recently, autonomous experimentation has emerged as a tool for accelerating design for properties that require physical experiments by combining automated experimentation and active learning.[16–22] However, not all fabrication and test procedures are readily

PROGRESS AND POTENTIAL

Many facets of mechanical performance evaluation require using specialized experiments that are slow and expensive. For example, when designing components for impact conditions such as the crumple zone of a car, testing is expensive and destructive and requires large samples. In this study, we explore whether comparatively simple experiments can provide insight into highly specialized performance such as in impact. We fabricated lattices using 3D printing and tested them under quasi-static compression, which is more general and accommodates smaller samples than does impact testing. Using a database accumulated using automated quasi-static testing, we trained a machine-learning model that predicts impact performance from quasi-static data alone. In addition to accelerating the design of impact-resistant structures for safety applications, this work more generally illustrates how easy-to-acquire experimental data can allow one to better select samples for specialized experiments.

suitable for automation. In these cases, it is crucial to maximize the degree to which all experimental data can be brought to bear while designing for a property of interest. Design of structures for impact performance is one such case, as impact tests are more resource intensive and less compatible with automation than quasi-static tests. Furthermore, in contrast to impact testing, in which testing properties (i.e., impactor mass, energy, and speed) are coupled in a manner that necessitates testing full-scale components, the strain rate in quasi-static uniaxial testing can be freely chosen, thus allowing researchers to test representative portions of the full-sized sample.

While the prospect of using knowledge from quasi-static testing to design for impact is attractive, the fundamental mechanics that allow one to connect performance across these two different testing regimes is not fully or sufficiently understood. A previous study found that quasi-static stress-strain curves of octet lattices (0.01 mm/s compression speed) exhibited similar trends to those observed during impact testing (20 m/s impactor speed) including the presence of a linear elastic regime followed by a stress plateau prior to densification.[23] However, oscillations were also noted during impact testing that were not present during quasi-static loading, and this was attributed to either inaccuracies in the force measurement or compression wave reflections inside the lattice structures. Nevertheless, the qualitative connection observed between quasi-static and impact testing supports the idea that a relationship between the two regimes may exist. Despite examples of studies that attempt to connect these regimes, a predictive connection between them remains elusive. To take advantage of latent relationships between testing regimes, a powerful approach is to seek data-driven models. Indeed, an area in machine learning that focuses on connecting different but related domains is transfer learning.[24–26]

Here, we hypothesize that quasi-static testing can become an effective predictor of impact performance by combining transfer learning to capture relevant features of the quasi-static measurements and automated experimentation to accumulate sufficient data to train the relevant models (Figure 1). Additionally, while the toughness of octet lattices, which have been classified as stretching dominated, have been previously studied,[11,27,28] bending-dominated lattices have garnered increasing interest for absorbing mechanical energy owing to the fact that they collapse at a nearly constant plateau stress.[3,29–31] To explore this hypothesis, we generate a parametric family of lattices and perform quasi-static measurements to collect force-displacement (*F-D*) curves for lattices with design $\vec{x}$, where x contains the geometric parameters that fully define the lattice. Then, we use unsupervised learning to identify the distinguishing features of the *F-D* curves. Next, we performed impact tests on lattices to measure the maximum acceleration, a_m, from each acceleration a versus time t curve. Using both a_m and *F-D*, we employ feature representation transfer learning to build a predictive model, $\hat{a}_m(\vec{F})$. In this way, we can predict impact performance using only quasi-static measurements in a manner that is potentially generalizable to other structures because it does not rely on any specific geometric parametrization of the design. To test this approach, we develop additional parametric families of lattices and explore the transferability of models to connect quasi-static measurements to impact performance across these families. Ultimately, we build a model using 812 quasi-static and 141 impact tests that is able to predict the performance of previously uncharacterized lattices to within 18%.

RESULTS AND DISCUSSION

The parametric octet design space

To explore the impact performance of lattice-based designs, we developed a parametric octet lattice (Figure 2A) that is defined by the maximum radii of the struts and

[1]Department of Mechanical Engineering, Boston University, Boston, MA, USA

[2]Soldier Protection Directorate, US Army Combat Capabilities Development Command Soldier Center, Natick, MA, USA

[3]Department of Materials Design and Innovation, University at Buffalo, Buffalo, NY, USA

[4]Department of Computer Science, Boston University, Boston, MA, USA

[5]Department of Biomedical Engineering, Boston University, Boston, MA, USA

[6]Division of Materials Science & Engineering, Boston University, Boston, MA, USA

[7]Physics Department, Boston University, Boston, MA, USA

[8]Lead contact

*Correspondence: efmorgan@bu.edu (E.F.M.), brownka@bu.edu (K.A.B.)

https://doi.org/10.1016/j.matt.2022.06.051

Please cite this article in press as: Gongora et al., Designing lattices for impact protection using transfer learning, Matter (2022), https://doi.org/10.1016/j.matt.2022.06.051

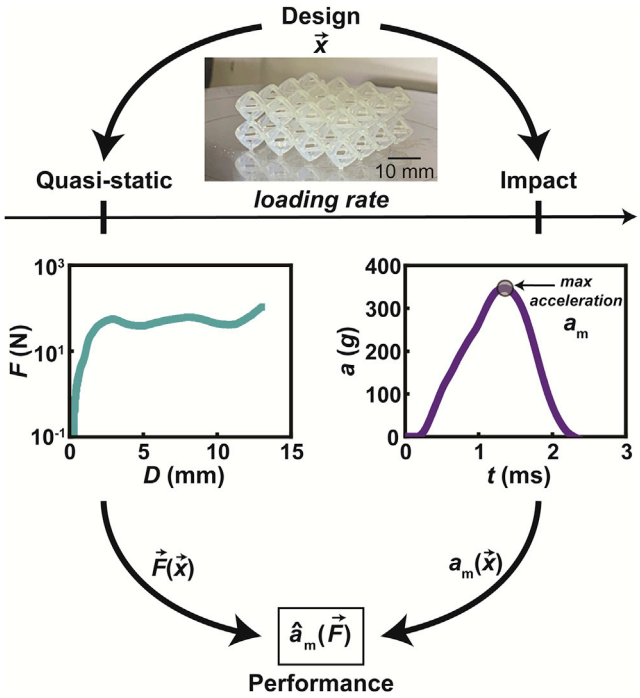

Figure 1. Using transfer learning to predict impact performance from quasi-static measurements
For a design $\vec{x}$, the force-displacement (*F-D*) curve can be obtained from quasi-static testing, and the acceleration-time (*a-t*) curve can be obtained from impact testing. Acceleration is reported in units of the gravitational acceleration *g*. Using both quasi-static measurements $\vec{F}(\vec{x})$ and impact performance, namely the maximum acceleration a_m in the *a-t* curve, a model $\hat{a}_m(\vec{F})$ can be built to predict a_m.

joints. The lattice designs were generated using custom code that adjusted the maximum radii of the lattice struts and joints to meet a target volume fraction (Figure S1).[32] It should be noted that this process is based on a weighting procedure that generates struts whose cross-sectional areas vary smoothly along their length and minimizes the sharpness of the corners at the joints where they intersect (details in experimental procedures). The generated designs were then exported as standard triangle language (STL) files for fabrication. Here, the lattice structures were designed to have a total height H = 19 mm, a length L = 38 mm, and a width W = 38 mm. The octet lattice was selected as a basis due to its use in previous studies on lightweight structures for applications in absorbing mechanical energy.[11,23,33–35] The octet unit cells had a lattice constant of 9.5 mm and were parametrized by $\vec{x} = (x_b, x_s, x_j)$, where x_b corresponds to the radius of struts that bend during uniaxial compression, x_s corresponds to the radius of struts that stretch during uniaxial compression, and x_j corresponds to the radius of the joints. All lattices were designed to a have a 10% volumetric fill fraction.

We initially studied three structures that varied in the degree to which stretching or bending would be expected to dominate their behavior. Specifically, under uniaxial compression, the oblique struts of an octet lattice bend and the horizontal struts stretch. Here, we modulate the relative contributions of bending and stretching by adjusting x_b and x_s which allows us to access bending-dominated octet lattices even though octet lattices are conventionally categorized as stretching dominated.[33,36,37] Three designs are shown that range from most resistant to stretching to least resistant to stretching (Figure 2B). For instance, design (I) is chosen to be highly stretching resistant by making x_s

Please cite this article in press as: Gongora et al., Designing lattices for impact protection using transfer learning, Matter (2022), https://doi.org/10.1016/j.matt.2022.06.051

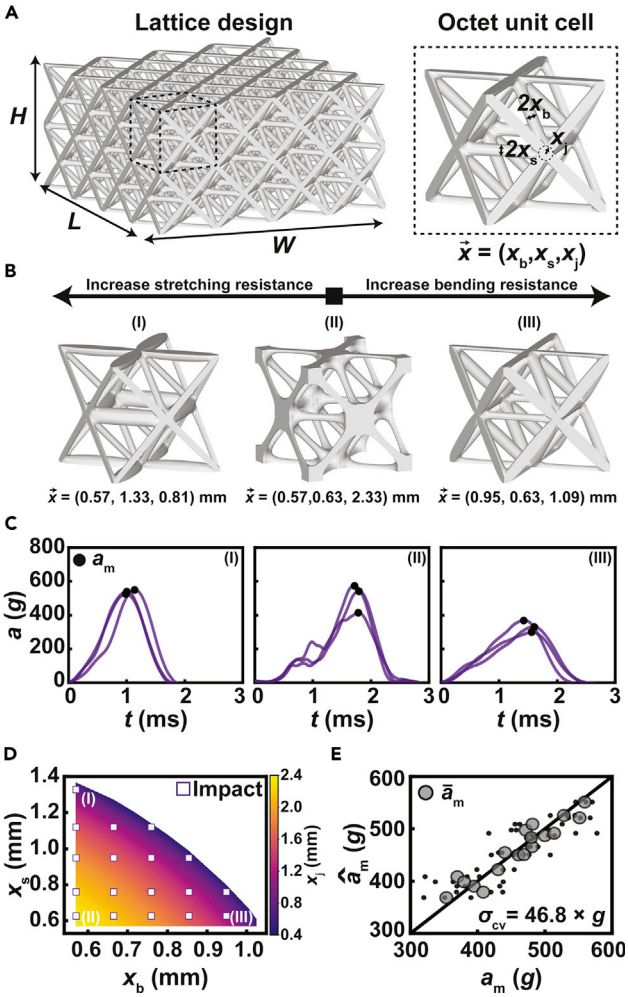

Figure 2. Parametric octet-based lattice designs for impact protection

(A) Samples for impact testing have length L, width W, and height H and are composed of repeating octet unit cells that are parametrized by $\vec{x} = (x_b, x_s, x_j)$, where x_b corresponds to the maximum radius of struts that bend during uniaxial compression, x_s corresponds to the maximum radius of struts that stretch during uniaxial compression, and x_j corresponds to the maximum radius of the joints.

(B) Three parametric octet designs (I), (II), and (III) that range from maximum resistance to stretching to maximum resistance to bending.

(C) Impact testing of samples of designs (I), (II), and (III) showing peak acceleration a_m from the a-t curves. Each panel shows testing results from three identically prepared samples.

(D) The parametric octet design space with markers that indicate the 18 designs that were measured using impact testing.

(E) The parity plot of $\hat{a}_m$ versus a_m where $\hat{a}_m$ comes from a Gaussian process regression (GPR) with root-mean-square error (RMSE) $\sigma_{CV} = 46.8 \times g$ calculated using leave-one-out cross-validation (CV). Gray dots show mean measured peak acceleration $\bar{a}_m$, and black dots show individual measurements of a_m.

to near its maximum allowed value. In contrast, design (II) features nearly equal x_b and x_s, correspondingly decreasing the importance of stretching. Finally, design (III) increases x_b to near its maximum achievable value to realize a structure with maximized bending resistance.

Samples based on designs (I), (II), and (III) were fabricated and tested. Three samples of each design were printed using stereolithography (SLA; Form 3 early 2019 model,

Please cite this article in press as: Gongora et al., Designing lattices for impact protection using transfer learning, Matter (2022), https://doi.org/10.1016/j.matt.2022.06.051

Formlabs) out of Durable Resin (product number RS-F2-DUCL-02, Formlabs) and impact tested using a drop tower impact testing system (CEAST 9350, Instron) with a 3.104 kg mass at 4.3 m/s impact velocity (Figure 2C). To aid in printing and removal, custom support structures were used (Figure S2). Additional information on the fabrication and testing methods can be found in the experimental procedures. Impact testing showed a rich array of subtle features, including two peaks in the *a-t* curve from samples based on design (II), which we attribute to the buckling of their slender struts during impact. Perhaps most importantly, a_m was observed to be lowest for the sample designed to have the largest bending resistance, i.e., those based on design (III), which is aligned with previous work suggesting that bending-dominated mechanics could be favorable for absorbing mechanical energy at lower peak accelerations.[29–31] Ultimately this means that design (III) is relatively high performing as it results in the lowest peak acceleration. While these observations are encouraging, they do not represent a sufficient exploration of this design space. Thus, we selected and tested 15 additional designs using a grid-based approach (Figure 2D). All additional selected designs were also fabricated in triplicate and tested for a total of 54 experimental measurements of a_m. Using x and a_m, we trained a predictive model $\widehat{a}_m(\overrightarrow{x})$ using Gaussian process regression (GPR) (Figure 2E). Details of this model are shown in the experimental procedures, but briefly, we selected a squared exponential covariance kernel with automatic relevance determination and a zero-mean function. The GPR was implemented in Python leveraging open-source software (http://sheffieldml.github.io/GPy/). The prediction accuracy of the model was determined by computing the root-mean-square error (RMSE) $\sigma_{CV} = 46.8 \times g$ using leave-one-out cross-validation (CV). We observed good agreement between a_m and $\widehat{a}_m$ considering that $\sigma_{CV} = 46.8 \times g$ is comparable to the $55 \times g$ standard deviation observed in quality control impact tests conducted throughout the experimental study (Figure S3).

Using quasi-static measurements to train a predictive model for impact performance

The use of quasi-static testing to study the mechanical behavior of materials and structures is ubiquitous in mechanics. Here, we hypothesize that transfer learning can identify characteristics of the *F-D* curve obtained from quasi-static testing that serve as predictors for impact performance. To test this hypothesis, we fabricated and conducted uniaxial quasi-static compression tests of samples based on designs (I), (II), and (III) using a universal testing machine (5965, Instron) at a loading rate of 2 mm/min (Figure 3A). Samples for quasi-static testing had a unit cell lattice constant of 9.5 mm, a H of 19 mm, an L of 19 mm, and a W of 19 mm. Interestingly, the *F-D* curves showed that samples based on design (III) exhibited the highest and smoothest plateau region after yielding. These quasi-static behaviors agree with predictions of post-yield plateau and softening in bending- and stretch-dominated structures, respectively.[29,36] The variations in force during the plateau region observed for samples based on designs (I) and (II) could indicate the buckling of struts during compression.

We hypothesize that, provided a sufficiently large database of measurements, transfer learning could allow one to connect quasi-static measurements and impact performance. Specifically, we propose a pipeline in which unsupervised learning is used to learn relevant features z from the quasi-static measurements and then combine these features with measured values of a_m to train a model to predict $\widehat{a}_m$ (Figure 3B). However, before embarking on this data-driven path, it is critical to obtain a sufficiently large quantity of data. Thus, we conducted quasi-static experiments of samples based on 653 unique design locations selected using a grid-based approach in

Please cite this article in press as: Gongora et al., Designing lattices for impact protection using transfer learning, Matter (2022), https://doi.org/10.1016/j.matt.2022.06.051

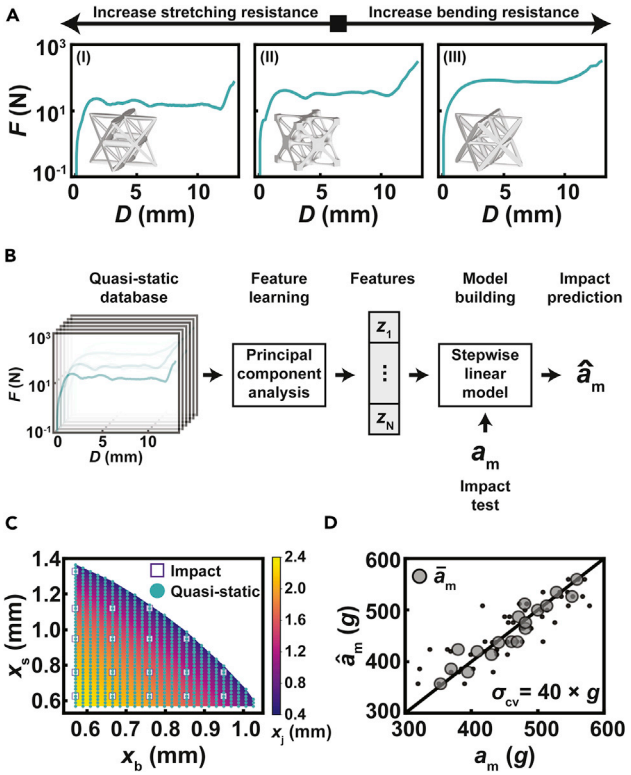

Figure 3. Predicting impact performance using quasi-static measurements via feature-representation transfer learning

(A) Quasi-static testing of three parametric octet samples based on designs (I), (II), and (III).

(B) Schematic of transfer learning pipeline to learn relevant features z of *F-D* curves that, together with a_m, can be used to train a predictive model $\hat{a}_m(z)$.

(C) The parametric octet design space where the square markers indicate the 18 designs tested in impact and circular markers indicate the 653 designs measured using quasi-static testing.

(D) Parity plot of $\hat{a}_m$ versus a_m where $\hat{a}_m$ is obtained from the transfer learning approach with forward stepwise linear regression model with $\sigma_{CV} = 40 \times g$.

the octet design space (Figure 3C). To increase experimental throughput, the samples for impact testing and quasi-static testing were printed in batches. Samples for impact testing were ordered in a three-by-three grid on the print baseplate (Figure S4A), and samples for quasi-static testing were ordered in a six-by-six grid arrangement on the print baseplate (Figure S4B). Quality control lattices and cylindrical samples were printed and tested for each quasi-static batch (Figures S5–S7). To collect this vast dataset, the quasi-static testing throughput was enhanced using custom automated experimentation hardware that leveraged robotic sample retrieval, handling, quasi-static testing, and data logging. This automated pipeline allowed for the collection of orders of magnitude more data than previously realized in related mechanical studies.[11,23,27,28]

Quasi-static data in hand, we sought to realize a transfer learning pipeline using a four-step process. (1) We first down sampled each *F-D* curve to 100 equally spaced *D* values from 0 to 13 mm to accommodate the non-uniform spacing from the instrument. The resolution of this down sampling was selected as a trade-off between computation time and adequately low loss of information (root-mean-square percentage error <2%) (Figure S8). Noting the wide range of *F* values in a given *F-D* measurement, we elected to learn on the logarithm of *F*. Additionally, since the

Please cite this article in press as: Gongora et al., Designing lattices for impact protection using transfer learning, Matter (2022), https://doi.org/10.1016/j.matt.2022.06.051

samples tested in quasi-static had a cross-sectional area that was a quarter the size of the lattices tested in impact, the forces measured during these tests were multiplied by four to determine the equivalent force measurements expected for quasi-static testing of a full-size sample. To explore whether this scaling led to systematic errors, we conducted six quasi-static compression experiments on quarter-size lattices and on full-size samples (Figure S9A). Not only were there minimal qualitative differences between the scaled curves, but the energy absorbed per unit volume exhibited no statistical difference ($p = 0.41$ for two-tailed t test) between the quarter-size samples and the full-size samples (Figure S9B). (2) We subsequently used principal-component analysis (PCA) on the log(F) dataset to build a featurizer to transform log(F) to z. It is important to note that z is determined with no knowledge of impact performance and is reflective of the variations and important features in quasi-static measurements. Additionally, not all z are important and should be considered to predict impact performance. (3) To select a subset of z for consideration in building models for impact performance, we selected the fewest components that have a cumulative explained variance >99% (Figure S10A), which results in N components for consideration. For these experiments, N was found to be 11. (4) Finally, forward stepwise linear regression was utilized to obtain the final predictive model. In brief, we computed linear models with k terms for $k = 1$ up to $k = N$ and computed the RMSE using CV for each k (Figure S10B). We then selected the optimal model as the k with the minimum σ_{CV}, here found to be $k = 6$ with $\sigma_{CV} = 40 \times g$. Limiting the number of terms using CV is designed to mitigate the potential for overfitting. The result of this four-step process was a final model defined as $\widehat{a}_m = \sum_0^k \beta_i z_i$ where β_i is the linear slope coefficient and $i = 0$ corresponds to a constant offset. This model results in good agreement between prediction and experiment (Figure 3D). We note that $\sigma_{CV} = 40 \times g$ is comparable to the $55 \times g$ standard deviation observed in quality control samples (Figure S3) and is lower than σ_{CV} computed using the GPR-based model (Figure 2E).

Testing the trained model for a different lattice family

From the octet lattice design space explored in the previous section, it was observed that octet designs that were more resistant to bending possessed superior performance. We therefore sought to explore a second family of lattices whose design would allow larger resistance to bending and allow us to test the model trained on octet data. Specifically, we chose octahedral lattices, which have been used in studies of energy absorption[38,39] and consist of octet unit cells without the tetrahedral struts.[33] The omission of these struts allows for larger strut diameters relative to those found in the octet designs. The octahedral lattice family considered in this study was also parametrized by $x = (x_b, x_s, x_j)$ where these are defined identically to how they were defined for the parametric octet lattices (Figure 4A). The unit cell lattice constant, volume frame, L, W, and H were the same for both octahedral and octet samples. To initially probe this design space, two distinct octahedral designs were tested under both quasi-static and impact conditions (Figure 4B). As with the octet samples, the design that was most resistant to bending, namely (V), possessed superior impact performance relative to design (IV), which was chosen to have maximized stretching resistance. These results motivate further exploration of the octahedral design space, since a_m measured for samples based on design (V) were, on average, 48% lower than the best-performing octet design.

While it was clear that octahedral lattices could outperform octet lattices during these impact tests, we sought to determine whether we could have predicted the performance of octahedral samples using the model trained on only octet data.

Please cite this article in press as: Gongora et al., Designing lattices for impact protection using transfer learning, Matter (2022), https://doi.org/10.1016/j.matt.2022.06.051

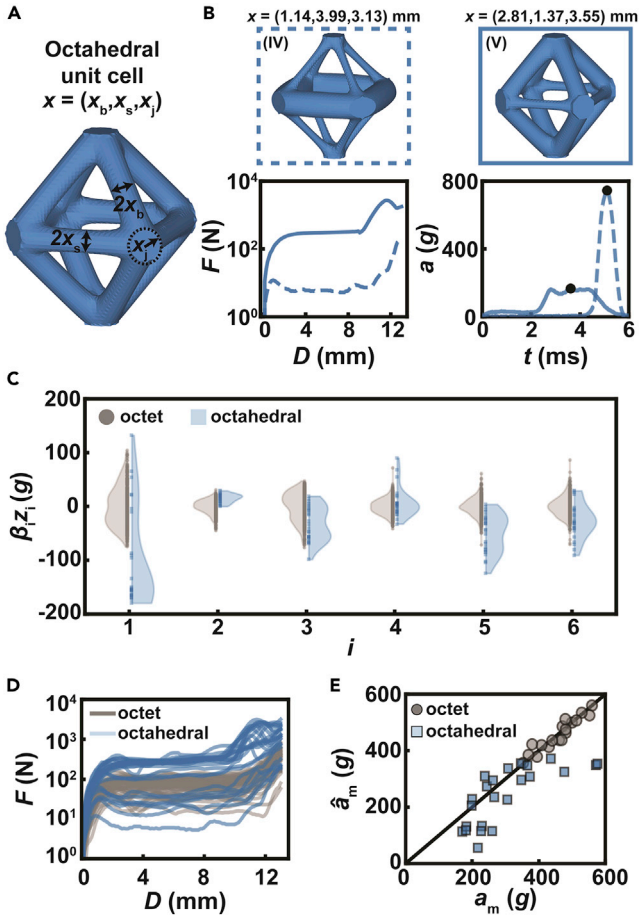

Figure 4. Evaluating the predictive ability of the octet-trained model using a parametric octahedral design space

(A) Definition of the geometry of the parametric octahedral unit cell.

(B) Quasi-static and impact testing of two distinct octahedral lattices based on a highly stretching resistant design (IV, dashed lines) and a highly bending-resistant design (V, solid lines).

(C) Violin plots of $\beta_i z_i$ versus i for octet and octahedral designs where β_i and z_i correspond to the model linear coefficient and selected principal component, respectively. Violin plots highlight the density of data and limited overlap between corresponding terms of the octet and octahedral lattices suggests predicting performance might be possible in some cases.

(D) Quasi-static *F-D* curves corresponding to the 18 octet and 26 octahedral designs that were tested in impact.

(E) Parity plot of $\hat{a}_m$ versus a_m for octet and octahedral designs using an octet-trained model.

The first question, however, is to determine whether the performance of the octahedral samples could be interpolated (rather than extrapolated) from the data from octets. To test this, we needed a representative set of quasi-static measurements from the octahedral design space. Thus, we measured samples based on 136 parametric octahedral designs using automated quasi-static testing. Next, these *F-D* measurements were transformed to *z* values using the octet-trained PCA featurizer. As the octet-trained model only relies upon k = 6 of these components, we compute the products $\beta_i z_i$, which each have units *g*, for each octahedral and octet sample to compare their distributions (Figure 4C). The $\beta_i z_i$ values computed for the octet samples were centered on zero, which is to be expected since the PCA was based on octet data. However, even though there is some overlap between the octahedral and octet data, many octahedral designs fall far outside the range defined by the

Please cite this article in press as: Gongora et al., Designing lattices for impact protection using transfer learning, Matter (2022), https://doi.org/10.1016/j.matt.2022.06.051

octet samples. The presence of some overlap suggests that the octet-trained model should have some predictive capability for octahedral designs.

To determine the degree to which octahedral impact performance can be predicted using the octet-based model, we selected 26 designs that span the parametric octahedral design space. There is reason to believe that the performance of these samples would extrapolate beyond octet samples as the corresponding *F-D* curves from quasi-static conditions of the octahedral designs tested under impact conditions exhibited both a substantially wider range of yield force compared with the octet lattices tested (Figure 4D). These 26 octahedral samples were also evaluated using impact testing to determine a_m, which can be compared with $\hat{a}_m$ as predicted by the octet-trained model (Figure 4E). Interestingly, several octahedral points are found near the parity line, suggesting reasonable prediction. However, we observe a degradation in prediction fidelity for especially low- or high-performing octahedral samples. Critically, while the absolute prediction accuracy is not high fidelity, the predicted rank of octahedral samples does appear to have reasonable correspondence with the measured rank. This is an important observation as not only are these octahedral data points not in the training set, but many fall outside the range (in terms of *z* or *F*) of data on which the model had been trained, and yet the model is providing valuable insight. Also, this process is only possible because this model takes *F* data as the input rather than the geometry of the sample.

To reconcile the mechanical results from the present study with classical understanding of impact mechanics, we compute the Janssen factor, or the ratio of the measured acceleration to the minimum possible acceleration. Classical understanding of foams suggests that a foam can either be too weak or too strong for a given impact condition and will exhibit a minimum Janssen factor *J* at a specified impact energy.[40] Plotting the impact results from the octet and octahedral study shows that, indeed, the best-performing components span a range of quasi-static energy absorbed from 4 to 9 J (Figure S11). The vast difference between this number and the 28 J energy dissipated during impact likely originates from strain-rate effects and that the quasi-static energy absorbed only considers pre-densification, while impact almost certainly reaches densification. Interestingly, the octahedral lattice designs span a wider range of both *J* and *U* relative to the octet lattice designs. Perhaps most importantly, however, is the variation of points along this curve, which illustrates that variations in component structure, even slight changes to the radii or curvature of struts, can have outsized effects on impact performance. This highlights the need for data-driven approaches to connect performance across these domains.

Building a general model for predicting impact performance

To build the most general possible model given the available data, we trained a model encompassing all quasi-static and impact data corresponding to both octet and octahedral designs (Figure 5A). First, we updated the PCA featurizer using all quasi-static data. The space was discretized into 100 *D* values as before. Here, we found that $N = 9$ components explained >99% of the variance (Figure S12A). After selecting components, we trained a forward stepwise linear regression model using all measurements of a_m. As before, the number of terms in this model was selected to minimize RMSE computed using CV (Figure S12B). Here, $k = 3$ terms were found to produce the best model. It is interesting to note that as the data became more diverse, fewer terms were needed to capture variance in the *F-D* curves themselves and the variation in impact performance. We attribute this to the model capturing more important trends in the larger dataset.

Please cite this article in press as: Gongora et al., Designing lattices for impact protection using transfer learning, Matter (2022), https://doi.org/10.1016/j.matt.2022.06.051

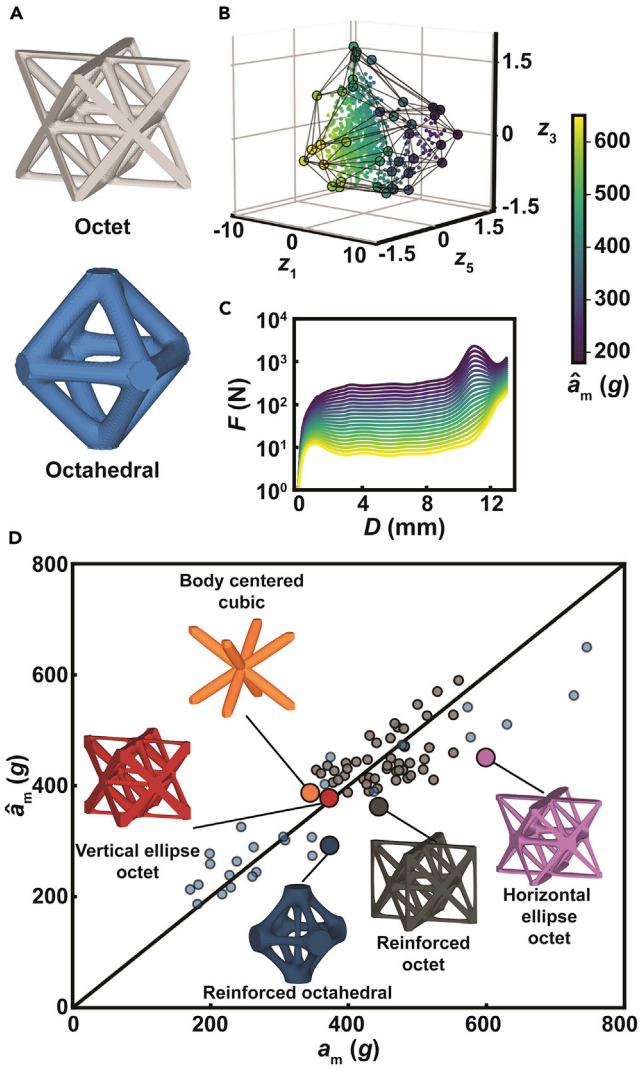

Figure 5. Validating the octet-octahedral based model using different lattices

(A) Illustrations of the octet and octahedral unit cells.

(B) Convex hull of the octet and octahedral designs based on *z* values from the three-term model obtained using forward stepwise linear regression. The color bar corresponds to $\hat{a}_m$ from this three-term model.

(C) Generated *F-D* curves using inverse PCA using *z* values along a linear trajectory from the points corresponding to the minimum $\hat{a}_m$ to the maximum $\hat{a}_m$.

(D) Parity plot of $\hat{a}_m$ versus a_m for octet, octahedral, and five different lattices using an octet-octahedral-trained model.

Given that three features were found to be ideal for predicting impact performance, we could readily visualize the impact performance within the feature space (Figure 5B). Importantly, this convex hull represents the domain for which the model has been trained and therefore can interpolate. A linear trajectory through this convex hull from the predicted worst-performing design (max $\hat{a}_m$) to the predicted best-performing design (min $\hat{a}_m$) can be generated to explore the relationship between quasi-static and impact performance. Specifically, taking points along this trajectory and generating their corresponding *F-D* curves using inverse PCA, we may visualize a series of *F-D* curves that trend from lowest performing to highest performing (Figure 5C). Interestingly, we observe that the *F-D* curves that correspond to

Please cite this article in press as: Gongora et al., Designing lattices for impact protection using transfer learning, Matter (2022), https://doi.org/10.1016/j.matt.2022.06.051

lower values of $\hat{a}_m$ also exhibited relatively high yield forces and minimal post-yield softening relative to those that correspond to higher values of $\hat{a}_m$. Strikingly, we observe a partial densification and subsequent softening at high strain for curves predicted to have lower values of $\hat{a}_m$. This partial densification and softening may be due to self-collisions and hyperelastic stiffening of bending-dominated struts at high strain. Regardless of its origin, the identification of this feature by a purely data-driven method indicates that transfer learning has the ability to draw connections between disparate domains in a manner that is able to help direct future in-depth mechanistic research.

To investigate the extent to which the model trained on octet and octahedral data can predict impact performance, we evaluated its prediction capabilities for five different lattices that were outside the training data: a reinforced octet, a reinforced octahedral, two different octets with struts that have elliptical cross-sections, and a body-centered cubic lattice. The structures designed from the five alternative designs had the same lattice constant, total size, and volume fraction as all previous octahedral and octet samples and were fabricated out of the same material. A parity plot showing the octet, octahedral, and all five alternative lattice designs reveals that the predictions for the five alternative lattices relative to the measured values are within reasonable agreement (root mean square percentage error = 18%) using the octet-octahedral-based model (Figure 5D). To emphasize, neither the PCA featurizer nor the predictive model $\hat{a}_m(z)$ have access to any information about the alternative designs, making these true validation samples.

From these results, two critical characteristics of the model were observed. First, the pipeline (Figure 3B) allows sequential updates as new data are acquired by updating both the lower dimensional feature space used to describe a design space and the model used to predict performance. This flexibility enables the utilization of previously collected data to connect properties such as relative rank of performance or absolute performance across design spaces. Secondly, the results show that the predictive power of the model built from data on the octet and octahedral lattices can extend to alternative lattice families. More generally, this observation suggests the ability of transfer learning to predict performance of novel designs for specialty applications.

Conclusion

This work combines several data-driven approaches to ultimately connect two distinct but related experimental responses using feature-representation transfer learning. First, a library of 812 uniaxial quasi-static measurements was collected through the use of AM and automated testing. This dataset was used to perform unsupervised learning to determine a set of features that capture the quasi-static performance. Then, a subset of these features was paired with 141 impact tests in order to build a model that predicts impact performance from quasi-static data. Not only can this model predict impact performance to within 13% (CV error), but it also predicts performance to within 18% for lattice families that are not included in any training (true validation error). This model, and the approach it exemplifies, has several implications for mechanical design and experimental research. First, this provides a facile method for using easy-to-obtain measurements to estimate difficult-to-measure properties. For example, the prediction of impact performance from quasi-static tests can vastly accelerate the design of impact structures. Second, and perhaps more importantly, the ability to examine the learned model to extract exemplars of high- and low-performance *F-D* curves has broader implications for enhancing researchers' abilities to learn the connections between mechanical

Please cite this article in press as: Gongora et al., Designing lattices for impact protection using transfer learning, Matter (2022), https://doi.org/10.1016/j.matt.2022.06.051

behaviors in different testing regimes. Third, while the application described here is primarily regarding lattice design, the approach provides a flexibility for applications in different fields, specifically those that have access to various characterization and measurement techniques that offer trade-offs in terms of time, cost, and fidelity. Furthermore, with the advancement of autonomous experimentation systems, approaches such as transfer learning could be introduced into the learning framework to further accelerate the pace of research by leveraging information from several sources to inform both decision-making and predictive modeling.

While the connection of two distinct but related experimental responses using feature representation and transfer learning highlight the role that machine learning can play in accelerating mechanical design, it also shines a spotlight on the role and consequences of model prediction errors in the data-driven design process. Firstly, the reported 13% cross-validation error of the final experimentally trained model should be compared with the inherent variation in the fabrication process. For instance, the best design is predicted to have a mean acceleration of 160 × g with a prediction error of 20 × g. This number should be compared with the 55 × g variation that was experimentally measured for the quality control samples. Indeed, in well-trained models, cross-validation error is expected to be commensurate with the measurement uncertainty, which in this case is dominated by variations in the performance in identically prepared samples. In this way, the cross-validation error is influenced by the measured variation in performance due to fabrication. Thus, this 13% cross-validation error highlights the need for more consistency in AM and advancements in *in situ* monitoring and control, metrology, and part inspection. Moreover, such cross-validation error can provide a useful input into any engineering analysis to aide in the selection of a factor of safety. Secondly, the reported 18% true validation error of this model refers to the error in predicting the performance of new lattice families not used in the training process. As was apparent when evaluating the octahedral lattices with the octet-trained model, even when such extrapolatory predictions do not provide quantitatively accurate results, the relative ranking provides highly actionable guidance for future design. Specifically, not only did the octet-trained model predict that octahedral samples would perform better, but it also pinpointed the region in parameter space that would correspond to the best performance. Thus, this type of prediction will aid in the selection of regions in design space to explore, keeping in mind that experimental evaluation in these regions will remain a critical part of the design loop. Indeed, we view this as an example of a data-driven design cycle in which designers use comparatively rapid and inexpensive measurements, namely quasi-static testing of representative samples, to screen vast libraries of potential structures and then use transfer learning to select candidates for more specialized impact testing.

EXPERIMENTAL PROCEDURES

Experimental procedures describing the design and fabrication of lattice samples, the quasi-static and impact testing protocol, and the predictive model building approach are found below.

Resource availability

Lead contact

Further information and requests for resources and reagents should be directed to and will be fulfilled by the lead contact, Keith A. Brown (brownka@bu.edu).

Materials availability

This study did not generate new unique reagents.

Please cite this article in press as: Gongora et al., Designing lattices for impact protection using transfer learning, Matter (2022), https://doi.org/10.1016/j.matt.2022.06.051

Data and code availability

All data needed to evaluate the conclusions in the paper are present in the paper and/or the supplemental information. The raw data can be accessed through www.kablab.org/data. Additional data related to this paper may be requested from the lead contact.

Design and fabrication of lattice samples

Lattice geometries were generated using custom design software written in MATLAB that is publicly accessible on kablab.org. The user inputs to the design software were the selected lattice family (e.g., octet lattice, reinforced octet lattice, octahedral lattice, or reinforced octahedral lattice), the bending strut radius x_b, the stretching strut radius x_s, and the volume fraction. In this study, the designs were constrained to have a target volume fraction of 10%. The lattices were generated using three base analog three-dimensional (3D) matrices corresponding to the lattice's features (bending struts M_b, stretching struts M_s, and joints M_j), as can be seen in the 2D example in Figure S1. M_b, M_s, and M_j were created by calculating the inverse of the signed distance field (i.e., the inverse of the distance of each voxel in the matrix from the skeleton of the feature of interest). Therefore, voxels that were closer to the feature of interest had a larger value, while points further from the feature of interest had a smaller value. M_b, M_s, and M_j were individually normalized so that their values ranged from zero to one (Figure S1B). A vector of scalar modifiers $\boldsymbol{w}$ was calculated by sampling representative points in M_b, M_s, and M_j that were x_b, x_s, and x_j distance away from their respective features of interest and using linear algebra to solve for the appropriate scalar values so that these sampling points each summed to a threshold α (Figure S1C). The locations of the sampling points were selected to decrease the influence of the other features, but ultimately the value at each sampling point was a combination of M_b, M_s, and M_j. The final lattice matrix M_f was created by summing M_b, M_s, and M_j with their weights adjusted by $\boldsymbol{w}$ and assigning material if the voxel value was above the threshold α, here taken to be 0.5 (Figures S1D and S1E). Each unique set of x_b, x_s, and x_j corresponds to a specific volume fraction. Here, a target volume fraction was designated, and x_j was a free variable that was then used to reach the target volume fraction. Because of this, the values of x_b and x_s were limited to a subset where the target volume fraction could be reached with a valid x_j, as seen by the boundaries in Figure 2D. The key benefits to this method over other methods are the vast variety of designs that can be created with a constant volume fraction with struts and joints that blend seamlessly, minimizing stress concentrations at the joint (Figure S1F).

After M_f was created, custom supports were added in the voxel space to aid in printing and removal of the parts (Figure S2A). Short, slender struts were extended downward from the bottom layer joints of the lattice, terminating in a solid square base to maximize contact area with the build plate (Figure S2B). The designs were then exported as STL files. The STL files were imported into commercial propriety print software (Pre-Form, Formlabs) to prepare the files for printing on an SLA 3D printer (Form 3 early 2019 model, Formlabs). The samples were manually arranged in a standard grid (Figure S4) with the custom support square placed flat on the build plate. All samples used in this study were fabricated from commercially available resin (Durable Resin, product number RS-F2-DUCL-02, Formlabs) with a layer thickness of 50 μm on a 14.5 × 14.5 cm^2 print baseplate.

To increase experimental throughput for impact testing, nine samples were printed in each production run. These samples for impact testing had an L of 38 mm, a W of 38 mm, and a H of 19 mm with four repeating unit cell designs along L and W and two

Please cite this article in press as: Gongora et al., Designing lattices for impact protection using transfer learning, Matter (2022), https://doi.org/10.1016/j.matt.2022.06.051

along *H*. The samples were ordered in a three-by-three grid on the print baseplate (Figure S4A). To further increase experimental throughput for quasi-static uniaxial compression testing, 36 samples were printed in each production run. These samples were a quarter of the full-size samples, resulting in samples with dimensions $L/2$, $W/2$, and H with two repeating unit cell designs along *L*, *W*, and *H*. To emphasize, the physical size of the unit cell was the same for both quasi-static testing and impact testing. Samples for quasi-static testing were ordered in a six-by-six grid arrangement on the print baseplate (Figure S4B).

After the printing process was completed, the samples, while still attached to the print baseplate, were moved to the washer (Form Wash, 8.6 L, Formlabs) filled with tripropylene glycol monomethyl ether (TPM) (Sigma-Aldrich) solvent to dissolve the remaining liquid resin on the samples. The samples were washed for 15 min, and, after washing, compressed air was used to blow out any remaining solvent. Next, the samples were manually submerged and rinsed for 30 s in a water tub. After rinsing, compressed air was used to blow out any remaining water. Samples were manually removed from the baseplate using a scraper, and lattice support structures were subsequently removed from the lattices using snippers. The lattice samples were arranged in the curing station (Form Cure, Formlabs) and cured for 75 min at 60°C. Finally, the samples were weighed prior to mechanical testing.

Quasi-static and impact testing of lattice structures

Quasi-static uniaxial compression proceeded at 2 mm/min on a universal testing machine (5965, Instron) with a force threshold of 4.5 kN. After necessary manual post-fabrication processing of the printed lattice structures, the quasi-static testing throughput was enhanced using custom automated experimentation that included automatic sample retrieval, testing, and data logging that all operated without human intervention. Since the samples tested in quasi-static were a quarter of the full-size lattices tested in impact, the forces measured during these tests were multiplied by four to determine the equivalent force measurements expected for quasi-static testing of a full-size sample.

To keep track of potential material property variations between print batches for samples tested under quasi-static conditions, a solid cylindrical sample that was 16 mm in height and 8 mm in diameter was printed with each production run. Throughout this process, a total of 20 cylindrical samples were printed, weighed, measured, and tested. Height and diameter measurements were taken by hand using digital calipers after the samples were cured. The mean recorded mass was 0.906 g with a coefficient of variation of 0.3% (Figure S5A). The mean height and diameter were calculated to be 15.93 (Figure S5B) and 7.98 mm (Figure S5C), respectively, with coefficients of variation of 0.4% and 0.4%, respectively. The absolute relative errors of the fabricated cylindrical samples with respect to the designed height of 16 mm and diameter of 8 mm were 0.4% and 0.3%, respectively.

The variation in the material property of the resin was also tracked from the quality control cylindrical experiments. From the measured force *F*-displacement *D* curves obtained during quasi-static compression testing, the stress σ-strain ε curves were calculated and used to derive the Young's modulus *E* and yield strength σ_y of each sample (Figure S6A). Here, *E* was computed to be the slope of the linear region of the σ-ε curve, and σ_y was measured as the stress at the 0.2% offset strain. For σ-ε curves with an observed initial toe region, *E* was measured from the slope of the linear region after the toe region, and σ_y was measured as the stress at the 0.2% offset strain with the toe being subtracted off to correct for the offset. From the

Please cite this article in press as: Gongora et al., Designing lattices for impact protection using transfer learning, Matter (2022), https://doi.org/10.1016/j.matt.2022.06.051

measurements, the mean E was calculated to be 570 MPa with a coefficient of variation of 12% (Figure S6B), and the mean σ_y was calculated to be 22 MPa with a CV of 12% (Figure S6C). The calculated coefficients of variation for SLA 3D printing with durable resin are comparable to our previous measured values of 9% coefficent of variation for E and 11% coefficient of variation for σ_y for cylindrical samples of equal dimensions printed from PLA from fused deposition modeling (FDM) 3D printing.[18]

In addition to the cylindrical quality control samples, a quality control lattice sample was also fabricated in each production run. A total of 23 quality control lattice samples were printed, weighed, and tested under quasi-static testing conditions. The number of successfully attained quality control cylindrical samples and quality control lattice samples differ by three samples due to human error. The design of the quality control lattices tested under quasi-static conditions was an octet lattice structure with design parameters (x_b, x_s, x_j) = (0.87, 0.87, 0.84) mm. The resulting F-D responses for all samples show a consistent shape (Figure S7A). From the mass measurements, the mean mass was calculated to be 0.83 g with a coefficient of variation of 2% (Figure S7B). Additionally, the toughness U of the samples was calculated as the area under the measured F-D curve. The mean U was calculated to be 16 J with a coefficient of variation of 6% (Figure S7C).

Impact testing was performed using a drop tower impact testing system (CEAST 9350, Instron Inc.) with a flat-ended steel impactor of mass equal to 3.104 kg. The drop-tower tests were conducted with a 4.3 m/s impact velocity. Full-sized samples with dimensions L, W, and H were tested under impact conditions. To assess the variation in performance among print batches, a quality control sample was included in each print job. The design of the quality control lattice was the same as the one selected for quasi-static testing. A total of 21 quality control samples were successfully printed, weighed, and tested. The mean mass of the samples was calculated to be 4.2 g with a coefficient of variation of 7% (Figure S3A). From the impact tests, the mean maximum acceleration $\bar{a}_m$ was found to be 460 × g, where g is the gravitational acceleration 9.81 $\frac{m}{s^2}$, with a CV of 12% (Figure S3B).

Building a predictive model for acceleration

From experimental measurements of a_m, a predictive model $\hat{a}_m(x)$ was built using GPR to model the property of interest in the design space $\vec{x} = (x_b, x_s)$. The covariance kernel $K(x, x')$ used in the GPR was a squared exponential kernel,

$$K(x, x') = \alpha^2 \exp\left(-\frac{1}{2}\sum_{j=1}^{d} \left(\frac{\left(x_j - x_j'\right)^2}{\beta_j^2} \right) \right), \qquad \text{(Equation 1)}$$

where K was parametrized by d + 1 parameters, namely α and β_j, and the dimensionality of the design space was d = 2. Here, β_j was comprised of d values. The parameters of the kernel and noise were optimized using maximum likelihood estimation. The GPR was implemented using Gpy, a Gaussian process framework written in Python (http://sheffieldml.github.io/Gpy/).

From the experimentally measured F-D response from quasi-static testing, the F measurements were down sampled to 100 equally spaced displacement locations over the range of the minimum displacement and a maximum displacement of 13 mm. The F measurements were down sampled because the F measurements for each design were collected with a differing total number of data points at non-uniform spacings, a consequence of the testing algorithm used by the universal

Please cite this article in press as: Gongora et al., Designing lattices for impact protection using transfer learning, Matter (2022), https://doi.org/10.1016/j.matt.2022.06.051

testing system. The number of equally spaced displacement locations was determined to be adequately suitable to represent the F with negligible loss of information (root mean square percentage error < 2%) (Figure S8). The maximum displacement of 13 mm was selected as the largest displacement measured for all samples in the study. Additionally, the logarithm of F was used as an input for further processing due to the wide range of F values in the F-D response (Figure S8). As a result, for a dataset with p samples, the matrix representing all the sampled force curves as log of F would be of size $p \times 100$. Using this matrix, we performed PCA to obtain a new set of features, namely the principal components z.[41]

Using both the experimentally collected a_m and z, we performed forward stepwise linear regression to build the model $\hat{a}_m(z)$.[25,26,42,43] A stepwise linear modeling was used for two reasons: (1) to select features from the available features from PCA and (2) to utilize Pearson's correlation coefficient as a metric for feature selection. Prior to employing the forward stepwise linear regression algorithm, a subset of z was selected where the number of selected components in the subset was based on the number of components with an explained variance greater than 99% (Figures S10A and S12A). Next, the regression procedure began by computing Pearson's correlation coefficient R between z and a_m. Then, the feature z_1 with the largest R^2 was selected as the first term in the regression model, specifically $\hat{a}_m(z) = \beta_1 z_1 + \beta_0$, where β_i and β_o corresponded to the coefficient of the selected feature and the intercept, respectively. The residuals were computed between a_m and $\hat{a}_m(z)$, and the feature most correlated with the residuals (i.e., the feature with the largest computed R^2) was selected as the next feature to add to the model, specifically $\hat{a}_m(z) = \beta_1 z_1 + \beta_2 z_2 + \beta_0$. This process was repeated until all components in the subset were selected. For example, if the number of components in the subset was 9, the process would terminate with a model as follows: $\hat{a}_m(z) = \beta_1 z_1 + \beta_2 z_2 + \cdots + \beta_9 z_9 + \beta_0$. The final model was selected based on the minimum RMSE calculated using CV based on 100 simulations and 20 folds (Figures S10B and S12B). To note, the observed RMSE was commensurate with the standard deviation observed in the impact performance of the quality control lattice as a measurement of the test error. The forward stepwise linear regression approach was implemented in Python using scikit-learn and SciPy open-source software.

Generating *F-D* curves in the convex hull

The minimum and maximum points, z_{min} and z_{max}, on the convex hull were selected based on the minimum $\hat{a}_m$ and maximum $\hat{a}_m$ from the model trained on both the octet and octahedral data. To generate a linear trajectory from the minimum $\hat{a}_m$ to maximum $\hat{a}_m$, the z values along the trajectory were computed using parametric linear equations, specifically $z_{traj} = z_{min} + q\,(z_{max} - z_{min})$, where $q \in [0, 1]$. The selected z values were the nine that corresponded to an explained variance >99%. Using inverse PCA, the F-D curves were constructed for 20 points along the trajectory including the minimum and maximum points.

SUPPLEMENTAL INFORMATION

Supplemental information can be found online at https://doi.org/10.1016/j.matt.2022.06.051.

ACKNOWLEDGMENTS

This work was supported by Google LLC, the Boston University Dean's Catalyst Award, the Boston University Rafik B. Hariri Institute for Computing and

Computational Science and Engineering (2017-10-005), the NSF (CMMI-1661412), and the US Army DEVCOM Soldier Center (contract W911QY2020002). Approved for public release: PR2022_30333. We also acknowledge support through the Boston University Photonics Center.

AUTHOR CONTRIBUTIONS

Conceptualization, all authors; methodology, all authors; software development, A.E.G. and K.L.S.; investigation, A.E.G. and K.L.S.; impact experiments, R.P., T.M.T., and T.J.L.; writing – review & editing, all authors.

DECLARATION OF INTERESTS

The authors declare no competing interests.

INCLUSION AND DIVERSITY

One or more of the authors of this paper self-identifies as an underrepresented ethnic minority in science. One or more of the authors of this paper self-identifies as a member of the LGBTQ+ community. One or more of the authors of this paper received support from a program designed to increase minority representation in science.

Received: February 9, 2022
Revised: May 12, 2022
Accepted: June 17, 2022
Published: July 19, 2022

REFERENCES

1. Clough, E.C., Plaisted, T.A., Eckel, Z.C., Cante, K., Hundley, J.M., and Schaedler, T.A. (2019). Elastomeric microlattice impact attenuators. SSRN Electron. J. *1*, 1519–1531. https://doi.org/10.2139/ssrn.3427465.

2. Lazarus, B.S., Velasco-Hogan, A., Gómez-del Río, T., Meyers, M.A., and Jasiuk, I. (2020). A review of impact resistant biological and bioinspired materials and structures. J. Mater. Res. Technol. *9*, 15705–15738. https://doi.org/10.1016/j.jmrt.2020.10.062.

3. Mueller, J., Matlack, K.H., Shea, K., and Daraio, C. (2019). Energy absorption properties of periodic and stochastic 3D lattice materials. Adv. Theory Simul. *2*, 1900081. https://doi.org/10.1002/adts.201900081.

4. Gu, G.X., Takaffoli, M., and Buehler, M.J. (2017). Hierarchically enhanced impact resistance of bioinspired composites. Adv. Mater. *29*, 1700060. https://doi.org/10.1002/adma.201700060.

5. Jia, Z., Yu, Y., Hou, S., and Wang, L. (2019). Biomimetic architected materials with improved dynamic performance. J. Mech. Phys. Solids *125*, 178–197. https://doi.org/10.1016/j.jmps.2018.12.015.

6. Qiao, P., Yang, M., and Bobaru, F. (2008). Impact mechanics and high-energy absorbing materials: review. J. Aerosp. Eng. *21*, 235–248. https://doi.org/10.1061/(asce)0893-1321(2008)21:4(235).

7. Zhu, F., Lu, G., Ruan, D., and Wang, Z. (2010). Plastic deformation, failure and energy absorption of sandwich structures with metallic cellular cores. Int. J. Prot. Struct. *1*, 507–541. https://doi.org/10.1260/2041-4196.1.4.507.

8. Andreassen, E., Lazarov, B.S., and Sigmund, O. (2014). Design of manufacturable 3D extremal elastic microstructure. Mech. Mater. *69*, 1–10. https://doi.org/10.1016/j.mechmat.2013.09.018.

9. Chen, D., Skouras, M., Zhu, B., and Matusik, W. (2018). Computational discovery of extremal microstructure families. Sci. Adv. *4*, eaao7005. https://doi.org/10.1126/sciadv.aao7005.

10. Gibson, I., Rosen, D., and Stucker, B. (2015). Additive manufacturing technologies. In International Journal of Sustainable Development and Planning, Second edition (Springer-Verlag New York). https://doi.org/10.1007/978-1-4939-2113-3.

11. Ling, C., Cernicchi, A., Gilchrist, M.D., and Cardiff, P. (2019). Mechanical behaviour of additively-manufactured polymeric octet-truss lattice structures under quasi-static and dynamic compressive loading. Mater. Des. *162*, 106–118. https://doi.org/10.1016/j.matdes.2018.11.035.

12. Yeo, J., Jung, G.S., Martín-Martínez, F.J., Ling, S., Gu, G.X., Qin, Z., and Buehler, M.J. (2018). Materials-by-design: computation, synthesis, and characterization from atoms to structures. Phys. Scr. *93*, 053003. https://doi.org/10.1088/1402-4896/aab4e2.

13. Zhang, J., Lu, G., and You, Z. (2020). Large deformation and energy absorption of additively manufactured auxetic materials and structures: a review. Compos. B Eng. *201*, 108340. https://doi.org/10.1016/j.compositesb.2020.108340.

14. Zhang, L., Feih, S., Daynes, S., Chang, S., Wang, M.Y., Wei, J., and Lu, W.F. (2018). Energy absorption characteristics of metallic triply periodic minimal surface sheet structures under compressive loading. Addit. Manuf. *23*, 505–515. https://doi.org/10.1016/j.addma.2018.08.007.

15. Shepherd, T., Winwood, K., Venkatraman, P., Alderson, A., and Allen, T. (2020). Validation of a finite element modeling process for auxetic structures under impact. Phys. Status Solidi Basic Res. *257*, 1900197. https://doi.org/10.1002/pssb.201900197.

16. Burger, B., Maffettone, P.M., Gusev, V.V., Aitchison, C.M., Bai, Y., Wang, X., Li, X., Alston, B.M., Li, B., Clowes, R., et al. (2020). A mobile robotic chemist. Nature *583*, 237–241. https://doi.org/10.1038/s41586-020-2442-2.

17. Epps, R.W., Bowen, M.S., Volk, A.A., Abdel-Latif, K., Han, S., Reyes, K.G., Amassian, A., and Abolhasani, M. (2020). Artificial chemist: an autonomous quantum dot synthesis bot. Adv. Mater. *32*, 2001626. https://doi.org/10.1002/adma.202001626.

18. Gongora, A.E., Snapp, K.L., Whiting, E., Riley, P., Reyes, K.G., Morgan, E.F., and Brown, K.A. (2021). Using simulation to accelerate autonomous experimentation: a case study using mechanics. iScience *24*, 102262. https://doi.org/10.1016/j.isci.2021.102262.

19. Gongora, A.E., Xu, B., Perry, W., Okoye, C., Riley, P., Reyes, K.G., Morgan, E.F., and Brown, K.A. (2020). A Bayesian experimental autonomous researcher for mechanical design. Sci. Adv. *6*, eaaz1708. https://doi.org/10.1126/sciadv.aaz1708.

20. Kusne, A.G., Yu, H., Wu, C., Zhang, H., Hattrick-Simpers, J., DeCost, B., Sarker, S., Oses, C., Toher, C., Curtarolo, S., et al. (2020). On-the-fly closed-loop materials discovery via Bayesian active learning. Nat. Commun. *11*, 5966. https://doi.org/10.1038/s41467-020-19597-w.

21. MacLeod, B.P., Parlane, F.G.L., Morrissey, T.D., Häse, F., Roch, L.M., Dettelbach, K.E., Moreira, R., Yunker, L.P.E., Rooney, M.B., Deeth, J.R., et al. (2020). Self-driving laboratory for accelerated discovery of thin-film materials. Sci. Adv. *6*, eaaz8867. https://doi.org/10.1126/sciadv.aaz8867.

22. Nikolaev, P., Hooper, D., Webber, F., Rao, R., Decker, K., Krein, M., Poleski, J., Barto, R., and Maruyama, B. (2016). Autonomy in materials research: a case study in carbon nanotube growth. npj Comput. Mater. *2*, 16031. https://doi.org/10.1038/npjcompumats.2016.31.

23. Tancogne-Dejean, T., Spierings, A.B., and Mohr, D. (2016). Additively-manufactured metallic micro-lattice materials for high specific energy absorption under static and dynamic loading. Acta Mater. *116*, 14–28. https://doi.org/10.1016/j.actamat.2016.05.054.

24. Li, X., and Fourches, D. (2020). Inductive transfer learning for molecular activity prediction: next-Gen QSAR Models with MolPMoFiT. J. Cheminf. *12*, 27. https://doi.org/10.1186/s13321-020-00430-x.

25. Pan, S.J., and Yang, Q. (2010). A survey on transfer learning. IEEE Trans. Knowl. Data Eng. *22*, 1345–1359. https://doi.org/10.1109/TKDE.2009.191.

26. Weiss, K., Khoshgoftaar, T.M., and Wang, D.D. (2016). A survey of transfer learning. J. Big Data. https://doi.org/10.1186/s40537-016-0043-6.

27. Lv, W., Li, D., and Dong, L. (2020). Study on mechanical properties of a hierarchical octet-truss structure. Compos. Struct. *249*, 112640. https://doi.org/10.1016/j.compstruct.2020.112640.

28. Xiao, L., Xu, X., Song, W., and Hu, M. (2020). A multi-cell hybrid approach to elevate the energy absorption of micro-lattice materials. Materials *13*, 4083. https://doi.org/10.3390/ma13184083.

29. Ashby, M.F. (2006). The properties of foams and lattices. Philos. Trans. R. Soc. A Math. Phys. Eng. Sci. *364*, 15–30. https://doi.org/10.1098/rsta.2005.1678.

30. Calladine, C.R., and English, R.W. (1984). Strain-rate and inertia effects in the collapse of two types of energy absorbing structure. J. Mech. Sci. *26*, 689–701. https://doi.org/10.1016/0020-7403(84)90021-3.

31. Wagner, M.A., Lumpe, T.S., Chen, T., and Shea, K. (2019). Programmable, active lattice structures: unifying stretch-dominated and bending-dominated topologies. Extreme Mech. Lett. *29*, 100461. https://doi.org/10.1016/j.eml.2019.100461.

32. Rumpf, R.C., and Pazos, J. (2012). Synthesis of spatially variant lattices. Opt Express *20*, 15263. https://doi.org/10.1364/OE.20.015263.

33. Deshpande, V.S., Fleck, N.A., and Ashby, M.F. (2001). Effective Properties of the octet-truss lattice material. J. Mech. Phys. Solids *49*, 1747–1769. https://doi.org/10.1115/1.4040409.

34. Messner, M.C. (2016). Optimal lattice-structured materials. J. Mech. Phys. Solids *96*, 162–183. https://doi.org/10.1016/j.jmps.2016.07.010.

35. O'Masta, M.R., Dong, L., St-Pierre, L., Wadley, H.N.G., and Deshpande, V.S. (2017). The fracture toughness of octet-truss lattices. J. Mech. Phys. Solids *98*, 271–289. https://doi.org/10.1016/j.jmps.2016.09.009.

36. Deshpande, V.S., Ashby, M.F., and Fleck, N.A. (2001). Foam topology bending versus stretching dominated architectures. Acta Mater. *49*, 1035–1040. https://doi.org/10.1016/s1359-6454(00)00379-7.

37. Dong, L., Deshpande, V., and Wadley, H. (2015). Mechanical response of Ti-6Al-4V octet-truss lattice structures. Int. J. Solid Struct. *60-61*, 107–124. https://doi.org/10.1016/j.ijsolstr.2015.02.020.

38. Meza, L.R., Zelhofer, A.J., Clarke, N., Mateos, A.J., Kochmann, D.M., and Greer, J.R. (2015). Resilient 3D hierarchical architected metamaterials. Proc. Natl. Acad. Sci. USA *112*, 11502–11507. https://doi.org/10.1073/pnas.1509120112.

39. Schaedler, T.A., Ro, C.J., Sorensen, A.E., Eckel, Z., Yang, S.S., Carter, W.B., and Jacobsen, A.J. (2014). Designing metallic microlattices for energy absorber applications. Adv. Eng. Mater. *16*, 276–283. https://doi.org/10.1002/adem.201300206.

40. Gibson, L.J. (1999). Cellular solids: structure and properties. In Cambridge Solid State Science Series, Second edition (Cambridge University Press), p. 1.

41. Abdi, H., and Williams, L.J. (2010). Principal component analysis. Wiley Interdiscip. Rev. Comput. Stat. *2*, 433–459. https://doi.org/10.1002/wics.101.

42. Mao, K.Z. (2004). Orthogonal forward selection and backward elimination algorithms for feature subset selection. IEEE Trans. Syst. Man Cybern. B Cybern. *34*, 629–634. https://doi.org/10.1109/tsmcb.2002.804363.

43. Wiegand, R.E. (2010). Performance of using multiple stepwise algorithms for variable selection. Stat. Med. *29*, 1647–1659. https://doi.org/10.1002/sim.3943.